CrystEngComm

Accepted Manuscript

ROYAL SOCIETY OF CHEMISTRY

www.rsc.org/crystengcomm

Hydrothermal synthesis and electrochemical properties of tin titanate nanowires coupled with SnO_2 nanoparticles for Li-ion batteries

Hongkang Wang,[§,‖] Man Wang,[†] Beibei Li,[‖] Xia Yang,[†] Klara Safarova,[‡] Radek Zboril,[‡] Andrey L. Rogach[†] and Michael K. H. Leung[§,*]

[§] Ability R&D Energy Research Centre (AERC), School of Energy and Environment, City University of Hong Kong, Hong Kong SAR

[‖] Center of Nanomaterials for Renewable Energy (CNRE), State Key Lab of Electrical Insulation and Power Equipment, School of Electrical Engineering, Xi'an Jiaotong University, Xi'an, China

[†] Department of Physics and Materials Science, City University of Hong Kong, Hong Kong SAR

[‡] Regional Centre of Advanced Technologies and Materials, Faculty of Science, Department of Physical Chemistry, Palacky University in Olomouc, Olomouc, Czech Republic

[*] To whom correspondence should be addressed. E-mail: mkh.leung@cityu.edu.hk

Abstract

Tin titanate nanowires coupled with SnO_2 nanoparticles have been prepared by combination of the hydrolysis of Sn(II) precursor and tin-to-hydrogen ion-exchange using layered hydrogen titanate nanowires as conformal templates under hydrothermal conditions. This synthetic strategy allows for incorporation of electrochemically active Sn into the layered titanate and simultaneous deposition of SnO_2 nanoparticles on the as-prepared tin titanate nanowires. When used as anode materials in lithium ion batteries, the tin titanate nanowires coupled with SnO_2 nanoparticles showed improved cycle performance and increased lithium storage capacity as compared with mesoporous SnO_2 nanoparticle aggregates and hydrogen titanate nanowires. Electrochemical study indicated that introduction of of SnO_2 nanoparticles supported on tin titanate can buffer the large volume changes during the Li-Sn alloying and dealloying process in the flexible

layered titanate nanostructures with large interlayer distance. Besides, these composite structures exhibited remarkably low (<0.5 V) voltage for Li insertion electrode in lithium ion batteries.

Introduction

Tin-based nanomaterials such as SnO_2, SnO, or metallic Sn have been considered as potential anode materials for lithium-ion batteries, due to their high theoretical specific storage capacity (SnO_2:~790 mAh/g;[1] SnO: ~875 mAh/g;[2] Sn: ~990 mAh/g[3]) as compared with that of commercial graphite (~372 $mAh \cdot g^{-1}$).[2-6] One Sn atom can accommodate upto 4.4 Li atoms to form $Li_{4.4}Sn$ alloy, which contribute to the high lithium storage capacities of tin-based materials. However, Li-Sn alloying-dealloying process also involves large volume changes (as high as 300%),[4] resulting in the drastic "electrochemical pulverization" of electrodes. This eventually leads to the electrode disintegration and fast capacity fading upon long term cycling.[5, 7, 8] In order to overcome this drawback, strategies have been developed by size, morphology and composition control of the active tin-based materials[1, 9-13] or their nanoscale mixing with carbon-based materials such as graphene[14] and carbon nanotubes.[15-20] Layered titanate has been regarded as a promising host for lithium-ion intercalation due to its open structure with a much larger interlayer spacing.[21, 22] However, to the best of our knowledge, tin titanates were rarely investigated as potential anode materials for the lithium ion batteries. Sn_2TiO_4[23] and zirconium tin titanate[24] are mostly prepared by solid-state reaction involving high temperature sintering, which typically results in large particles with poor compositional homogeneity and not easy to be controlled structural morphologies. Recently, Beenakumari *et al*[25] reported co-precipitation synthesis of $SnTiO_3$ nanopowders, and Tsai *et al*[26] demonstrated incorporation of Sn^{2+} into the titanate nanotubes.

Herein, we prepared tin titanate nanowires coupled with well-dispersed SnO_2 nanoparticles, using hydrogen titanate nanowires as template precursors for hydrothermal reaction. At the same time, Sn ions from the precursor solutions are ion-exchanged with hydrogen to form tin titanate. This novel composite structure showed better cycle performance and higher lithium storage capacity than porous SnO_2 spheres and hydrogen

titanate nanowires, when applied as anode materials in lithium ion batteries. The atomic-scale incorporation of tin ions into titanate wires combined with well-dispersed SnO_2 nanoparticles tolerate volume changes due to the smaller atom number in the unit surface area and the large interlayer distances in the flexible titanate structures, which contributed to their better cycle performance.

Experimental section

Materials Fabrication. Chemicals including tin(II) chloride dihydrate ($SnCl_2 \cdot 2H_2O$, Sigma-Aldrich), sodium hydroxide (NaOH, Sigma-Aldrich), and P25 TiO_2 (Degussa), were used as received. Titanate nanowire precursors were prepared by alkaline hydrothermal method and successive ion-exchange synthesis, according to our previous reports.[1, 27] In a typical synthesis, 1.5 g P25 TiO_2 was dispersed in 80 mL 10M NaOH aqueous solution, followed by hydrothermal treatment at 180 ^oC for 48 h. Sodium titanate (Na-titanate, $Na_2Ti_3O_7$) nanowires were obtained by washing the collected white precipitate with distilled water until the pH reached ~7. Hydrogen titanate (H-titanate, $H_2Ti_3O_7$) nanowires were obtained by exchanging Na^+ ions in the Na-titanate with protons in a dilute HCl aqueous solution for one week, which was followed by washing with water until the pH reached ~7 and drying at 90 ^oC overnight. Tin titanate (Sn-titanate, $SnTi_3O_7$) nanowires coupled with SnO_2 nanoparticles were prepared by hydrothermal treatment of H-titanate nanowires in $SnCl_2$ aqueous solution. In a typical synthesis, 200 mg H-titanate nanowires were dispersed in 30 mL distilled water, and 0.67 g $SnCl_2 \cdot 2H_2O$ were added. The resulting yellow suspension was stirred for 1h at room temperature, and subsequently hydrothermally treated at 180 ^oC for 24h in a 50-mL Teflon-lined stainless steel autoclave. Porous SnO_2 spheres were prepared by hydrothermal treatment of $SnCl_2$ aqueous solutions containing 0.67 g $SnCl_2 \cdot 2H_2O$ in 30 mL water at 180 ^oC for 24 h. By lowering the introduced amount of H-titanate nanowire (from 200 mg to 100, 50, 20 mg), porous SnO_2 spheres have been produced, mixed with tin titanate nanowires. All the precipitates were washed with distilled water, collected by centrifugation for several cycles until the pH reached ~7, and dried at 90 ^oC overnight.

Structural Characterization. A Philips X'pert X-ray diffractometer (XRD) was applied to examine the phase structures, using Cu K α radiation (λ = 1.5418 Å) with an operating voltage of 40 kV and a current of 30 mA. Scanning electron microscopy (SEM) was used to characterize morphologies of the products, using a Philips XL30 FEG SEM. Transmission electron microscopy (TEM) was carried out on a Philips CM 20 and a JEOL JEM2100F TEM. HRTEM images were recorded on a high-resolution transmission electron microscope FEI Titan G2 60-300 kV (X-FEG, accelerating voltage of 300 kV). High angle annular dark field (HAADF) scanning transmission electron microscopy (STEM) study was carried out at 300 kV, combined with the use of an energy dispersive X-ray spectroscopy (EDS) spectrometer for the elemental analysis. X-ray photoelectron spectroscopy (XPS, Physical electronics PHI-5802) was used to determine the surface composition and chemical state of Sn. The specific surface areas of the products were measured by nitrogen adsorption-desorption isotherms at 77 K according to the Brunauer-Emmett-Teller (BET) method by using an Autosorb iQ-MP Surface Area and Pore Size Analyzer (Quantachrome Instruments).

Electrochemical Characterizations. Electrochemical measurements were performed using CR2032 coin cells. The electrodes were prepared by spreading a paste composed of 70 wt% active materials (porous SnO_2 spheres, H-titanate nanowires, or SnO_2 coupled tin titanate nanowires), 20 wt% acetylene black and 10wt % polyvinylidene fluoride on a copper foil current collector, followed by drying in a vacuum oven at 120 ^oC overnight. Lithium foil was used as a counter electrode, and a Cellgard 2400 microporous membrane as a separator. An electrolyte consisted of 1 M $LiPF_6$ dissolved in ethylene carbonate /dimethyl carbonate (1:1 in volume). The cells were tested on a battery test system (LAND-V34, Land Electronic Co., Ltd., Wuhan) at constant discharge and charge current densities of 100 mA/g in voltage window of 0.01-2.5 V at room temperature. Cyclic voltammetry (CV) measurements were performed on a Zahner IM6 electrochemical station in the 0.01-3.0 V window at a scan rate of 0.1 mV/s. Specific capacity is reported related to mass of the active materials such as porous SnO_2 spheres, H-titanate nanowires, or tin titanate nanowires coupled with SnO_2 nanoparticles.

Results and discussion

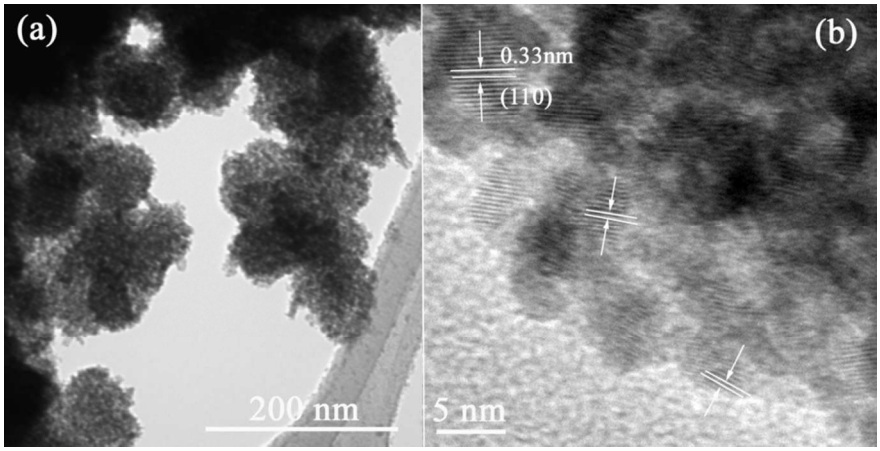

Figure 1. (a) TEM and (b) HRTEM images of mesoporous SnO_2 spheres obtained by hydrothermal treatment of $SnCl_2$ aqueous solution at 180°C for 24 h.

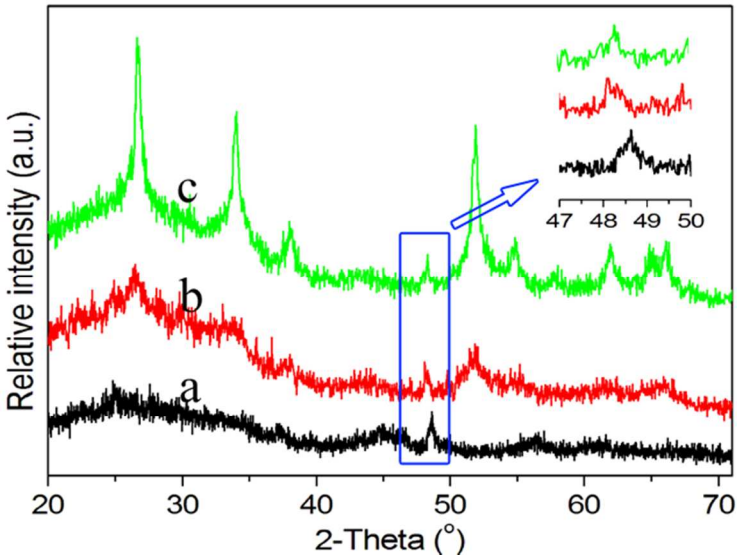

Figure 2. XRD patterns of H-titanate nanowire precursors (a) and SnO_2 coupled Sn-titanate nanowires obtained by introducing different amount of H-titanate nanowires (b: 200 mg; c: 100 mg).

As shown in Figure 1a, mesoporous SnO_2 spheres composed of loosely bound nanoparticles were obtained by hydrothermal treatment of aqueous $SnCl_2$ solutions.

HRTEM image (Figure 1b) reveals that SnO_2 nanocrystallites with size of 5~10 nm are aggregated with random orientations. Lattice spacing of 0.33 nm can be clearly observed, corresponding to (110) plane of SnO_2. Phase and morphology of the products can be affected by introducing different amount of H-titanate nanowires into the $SnCl_2$ aqueous solutions. Porous SnO_2 spheres mixed with tin titanate nanowires were produced by introducing small (20 to 100 mg) amount of H-titanate nanowires (Figure S1). XRD patterns presented in Figure 2 reveal that as-prepared H-titanate nanowires are poorly crystalline $H_2Ti_3O_7$ with monoclinic structure, according to previous reports.[27, 28] We note that due to their structural similarity, H-titanate nanowires can readily be transformed into wire-like anatase TiO_2 nanoparticle aggregates under hydrothermal treatment, when no other reactants are present in the reaction mixture (Figure S2).[1] However, H-titanate does not transform into anatase TiO_2 under hydrothermal treatment in aqueous $SnCl_2$ solution. As indicated by XRD patterns (Figure 2a *vs* 2b and 2c), no peaks can be indexed to TiO_2 phase. Instead, a peak present at $2\theta=48.5^o$ can be indexed to titanate structures, which undergoes shift to small diffraction angles, indicating the enlargement of crystal lattice due to the incorporation of larger Sn ions into the layered H-titanate structures through ion-exchange. Moreover, other diffraction peaks emerged after hydrothermal reaction with their intensity depending on the introduced amount of H-titanate nanowires, which can be indexed to tetragonal SnO_2 (cassiterite, JCPDS#41-1445). As shown in Figure S3, XRD patterns reveal that incorporation of Sn ions in the titanate lowers the annealing temperature for titanate-to-rutile phase transition.

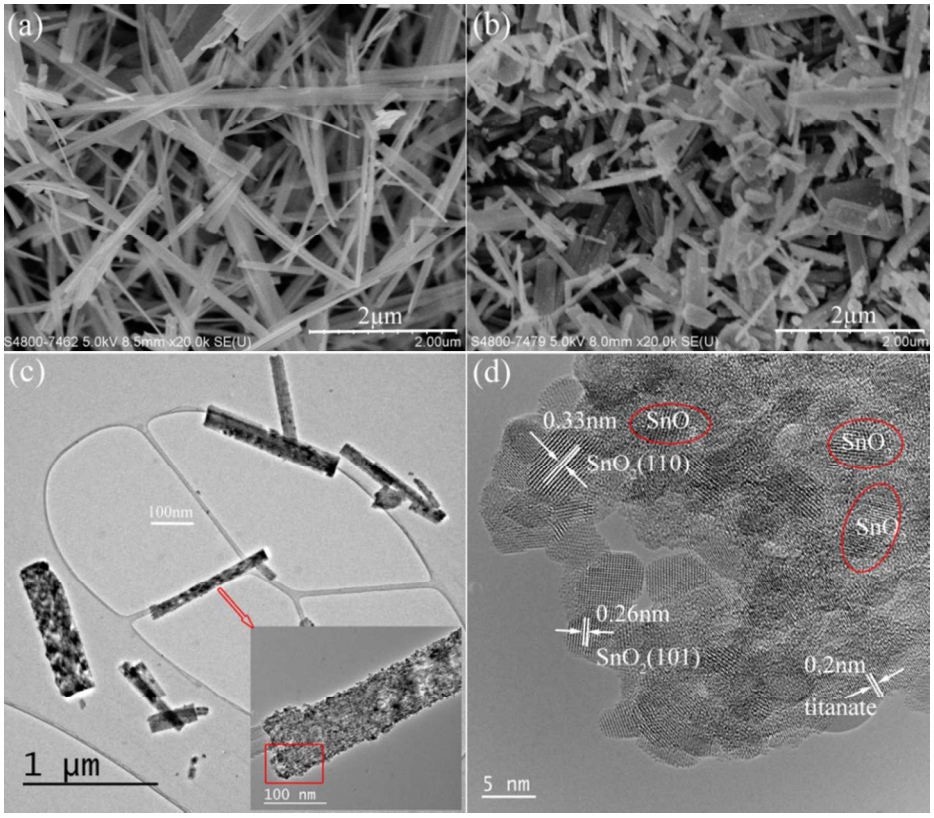

Figure 3. SEM images of (a) H-titanate nanowire precursors and (b) SnO_2 coupled Sn-titanate nanowires obtained by introducing 200 mg H-titanate nanowires into the hydrothermal reaction. (c) TEM image of SnO_2 coupled Sn-titanate nanowires with inset showing the corresponding enlarged TEM image. (d) HRTEM image of a fragment of single nanowire from (c).

Figure 3a shows the SEM image of H-titanate nanowires, with diameters of 20~150 nm, lengths of several micrometers (1~10 μm), and very smooth surface. After hydrothermal treatment in aqueous $SnCl_2$ solution, tin titanate nanowires coupled with SnO_2 nanoparticles were obtained. The wire-like morphology of the products was maintained, but wires appear to be broken into much shorter structures (Figure 3b, c). HRTEM image of a single wire reveals that the tin titanate nanowires are coated on the surface by numerous SnO_2 nanoparticles with size of just few nanometers (5~10nm) (Figure 3d). Their lattice distances of 0.26 nm and 0.33 nm can be assigned to (101) and (110) planes of SnO_2, respectively. HAADF image and corresponding EDS maps (Figure 4) taken from the single wire (Figure 4a) confirm the presence of Sn and Ti elements and their

relatively uniform distribution within the as-prepared tin titanate nanowires. Figure S4 shows the XPS survey spectra of H-titanate and Sn-titanate: new peaks belonging to Sn appeared after hydrothermal reaction, while Ti and O peaks were present in both samples before and after hydrothermal reaction without apparent shift. Due to the small difference in binding energies for Sn^{4+} and Sn^{2+}, it is a challenge to distinguish them by XPS. In our previous related studies,[1, 29-31] room-temperature ^{119}Sn Mössbauer spectra were used to determine the oxidation state of Sn element, and it was found that Sn^{2+} ions as self-dopants existed in the as-prepared SnO_2 product when using $SnCl_2$ as tin source.

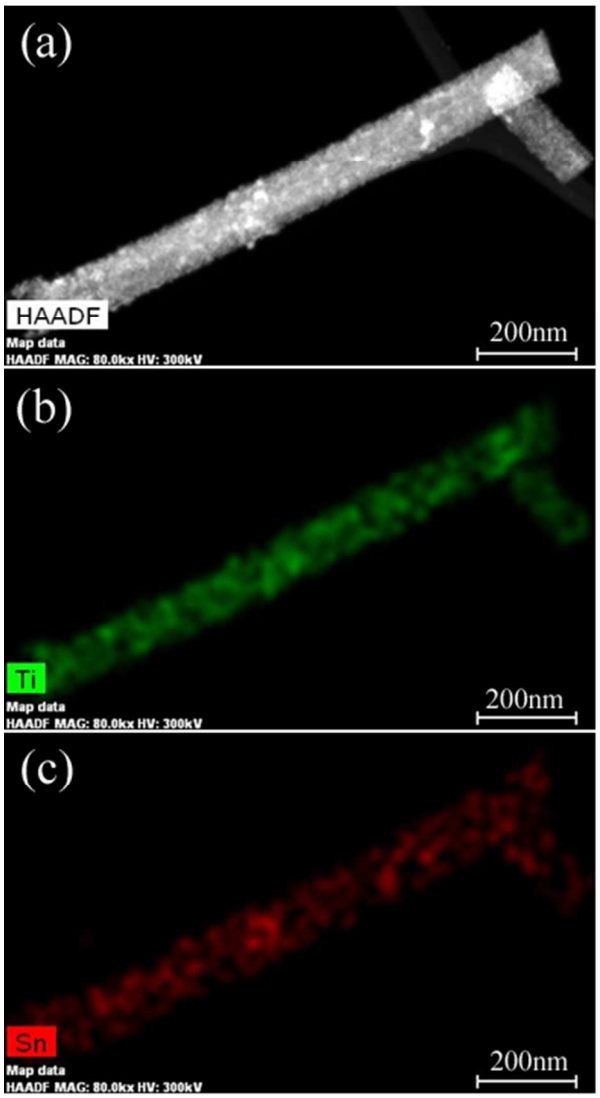

Figure 4. (a) HAADF image of tin titanate nanowires coupled with SnO_2 nanoparticles and corresponding EDS maps of (b) Ti and (c) Sn element distributions within the single nanowire.

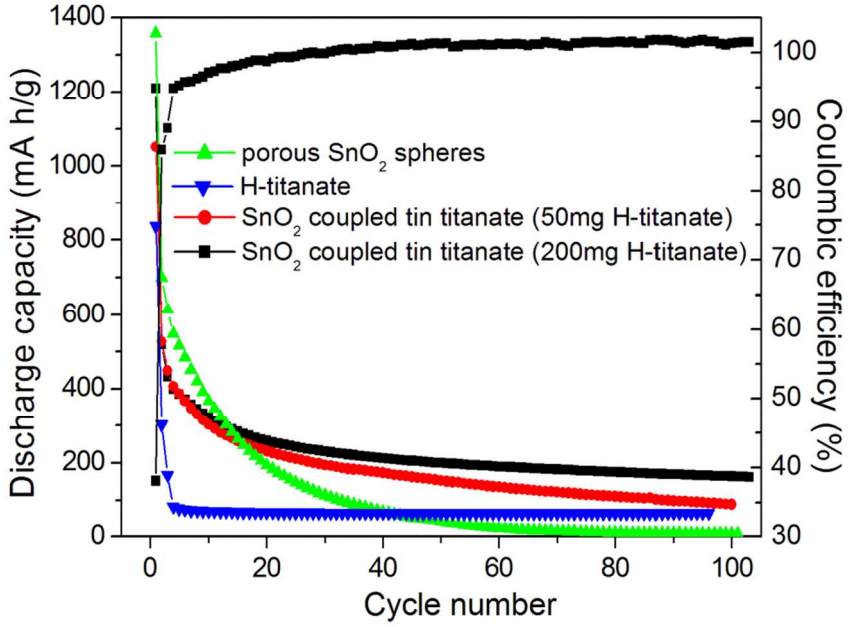

Figure 5. Cycle performance of porous SnO_2 spheres (green), H-titanate nanowires (blue) and SnO_2 coupled tin titanate nanowires (50 mg H-titanate precursor, red) at 100 mA/g in the voltage range 0.01-2.5 V. The Coulombic efficiency for SnO_2/tin titanate nanowires (200 mg H-titanate precursor) is also shown (black).

Electrochemical properties of the products were investigated in coin cells using lithium foil as the counter electrode. Figure 5 compares the cycle performances of porous SnO_2 spheres, H-titanate nanowires, and SnO_2 coupled tin titanate nanowires. Porous SnO_2 spheres undergo fast capacity fading with a value of 41 mA h/g after 50 cycles, which results from the electrochemical pulverization of SnO_2 materials due to the large volume changes during the Li-Sn alloying and dealloying,[4] while H-titanate nanowires deliver a stable discharge capacity of ~65 mA h/g. Tin titanates nanowires coupled with SnO_2 nanoparticles show increased discharge capacity and better cycle performance, which are dependent on the introduction amount of H-titanate nanowire precursors. At higher H-titanate content (200 mg), the as-prepared SnO_2 coupled tin titanate nanowires deliver a stable discharge capacity of 170 mA h/g even after 100 cycles, with Coulombic efficiency as high as 100%. At lower H-titanate content (50 mg), there were separated SnO_2 spheres present besides the SnO_2 nanoparticle coupled tin titanate nanowires

(Figure S2). This composite structure shows better capacity retention (~85 mA h/g after 100 cycles) than the pure SnO_2 (~5 mA h/g after 100 cycles) but worse than that of SnO_2 nanoparticles coupled tin titanate nanowires with less independent SnO_2 spheres (~170 mA h/g after 100 cycles). The fast capacity loss can be attributed to the pulverization of separated SnO_2 spheres in the composite structures. With introduction of H-titanate nanowires in the $SnCl_2$ precursor solutions, tin atoms were exchanged into the interlayers of TiO_6 octahedron layers in H-titanate nanowires, with simultaneous formation of well separated SnO_2 nanoparticles attached on the surface of tin titanate nanowires. BET surface area analysis reveals that aggregated SnO_2 particles show a large surface area of 133 m^2/g and a small average pore size of 1.7 nm (Figure S5), which deceases to 100 m^2/g and 48 m^2/g when 20 mg and 200 mg H-titanate nanowires were introduced in the precursor solutions, while the average pore sizes increases from 9.0 nm to 23.9 nm, respectively. Thus, isolated nanosized SnO_2 crystallites coupled to titanate nanowires with loose packing can tolerate larger volume changes than their agglomerates and facilitate the electrolyte penetration. On the other hand, incorporation of tin atoms into layered titanate nanostructures not only allow for the lithium storage but also buffer the unit cell volume changes during alloying-dealloying reactions, owing to the large interlayer distances and the flexibility of titanate nanostructures.[28]

Figure 6 shows cyclic voltammograms of the as-prepared and post-preparatively annealed (600 ^oC in air for 6h) SnO_2 coupled tin titanate nanowires at a scan rate of 0.1 mV/s in the voltage range 0.01-3.0V. Figure 6a compares first CV cycles of SnO_2 coupled tin titanate nanowires and Ti-doped SnO_2[1] obtained from H-titanate nanowires as sacrificial templates. Two broad reduction peaks at around 1.5 V and 1.0 V are present in the SnO_2 coupled tin titanate nanowires, which exhibit slight shift to large voltage and can be attributed to the irreversible formation of solid electrolyte interface (SEI: $Li^+ + e^-$ + electrolyte → SEI(Li)) and Li_2O ($SnO_2 + 4Li^+ + 4e^- \rightarrow Sn + 2Li_2O$).[9] The sharp reduction peak located at around 0.2V in all three samples corresponds to the alloying reaction between Sn and Li ($Sn + xLi^+ + xe^- \leftrightarrow Li_xSn$, $0 \leq x \leq 4.4$). [32] The corresponding oxidation peak located at around 0.5V is clearly observed and preserved the profiles in the following several cycles (Figure 6b), indicating the alloying reaction between Sn and Li is highly reversible. We note that another anodic peak is located in the range of 1.0-

1.8 V in both as-prepared SnO_2 coupled tin titanate nanowires and Ti-doped SnO_2 samples, which has been previously reported for number of SnO_2 electrodes.[1, 9, 33] Demir-Cakan et al attributed this peak to re-oxidation of Sn,[9] while Yang et al assigned it to the reactions on the electrode/electrolyte interface at the initial stage of electrochemical scan.[32] Our experiments show that both the broad reduction peak at around 1.5 V and the oxidation peak in the range of 1.0-1.8 V almost disappear in the annealed sample (Figure 6a), or gradually disappear in the subsequent several cycles for as-prepared samples (Figure 6b). These results further confirm the presence of some surface defect-catalyzed reactions among adsorbates/electrode/electrolyte interface, relating to successive activation process of the electrode in the initial several cycles.[32] Most importantly, there are no peaks which can be indexed to TiO_2, which further confirms that the ion exchange of Sn ions into the H-titanate nanowires inhibits the titanate-anatase phase transition, and indicates the high stability of tin titanate nanowires under hydrothermal condition.

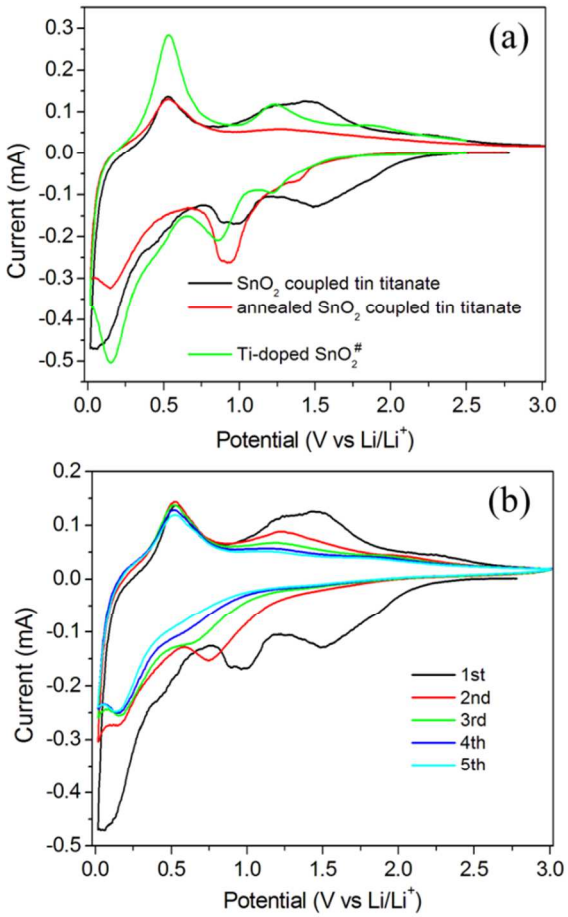

Figure 6. (a) First cycle of cyclic voltammograms of the as-prepared and post-preparatively annealed (600 ^{o}C in air for 6h) SnO_2 coupled tin titanate nanowires, compared to Ti-doped SnO_2 nanowires from Ref.[1]. (b) The initial five cyclic voltammograms of as-prepared SnO_2 coupled tin titanate nanowires.

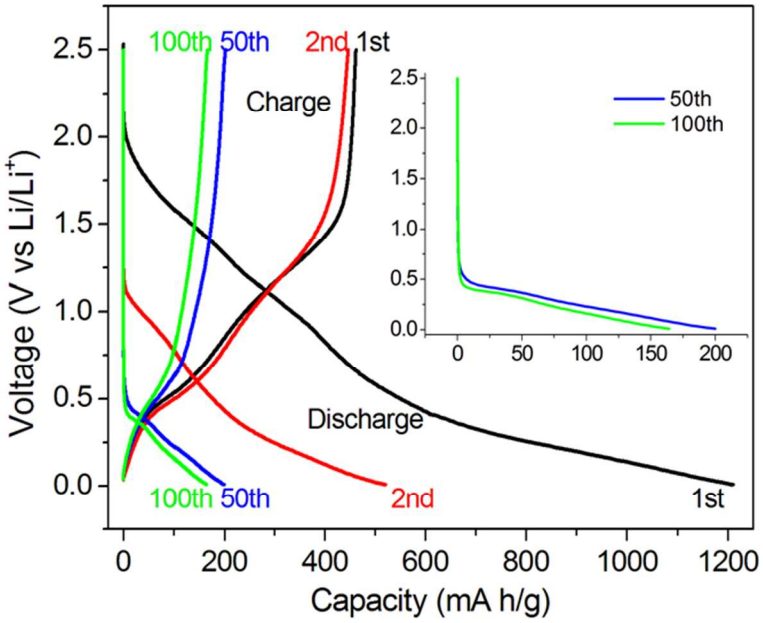

Figure 7. Charge–discharge voltage profiles of as-prepared SnO_2 coupled tin titanate nanowires at different current densities (1st to 2nd: 50 mA/g; 3rd to 100th: 100 mA/g). Inset shows the enlarged discharge profiles of 50th and 100th cycle.

Figue 7 shows the discharge/charge curves of as-prepared SnO_2 coupled tin titanate nanowires. The first discharge profile above 1.0 V (*versus* Li/Li$^+$) is higher than that of pure SnO_2 electrodes typically reported,[1, 5, 9-11, 13] which disappears in the second cycle. This may correspond to reduction of tin titanate to form Li_2O and metallic Sn, in addition to the irreversible reduction of SnO_2. The first discharge and charge process is characterized by specific capacity of ~1200 mA h/g and ~450 mA h/g with Coulombic efficiency of ~39%, indicating the large specific capacity loss due to the formation of SEI layer on the electrode and Li_2O.[34] Besides, the Li-Sn alloying-dealloying reactions generally occur below 1.0 V,[9] while our discharge profiles show that the Li insertion into as-prepared SnO_2 coupled tin titanate predominately happens below 0.5 V, which is remarkably low as compared to values reported in literature.[33-35]

Conclusions

We have demonstrated hydrothermal synthesis of tin titanate nanowires coupled with SnO_2 nanoparticles through hydrolysis, crsytallization of Sn(II) precursor and tin-hydrogen ion-exchange in the layered hydrogen titanate nanowire templates. Incorporation of Sn ions into titanate inhibited the titanate-to-anatase phase transition under hydrothermal treatment. SnO_2 nanoparticles were evenly distributed on the surface of titanate nanowires, and Sn ions were simultaneously incorporated into the layered titanate matrix. These structural characteristics help to accommodate large volume changes during Li-Sn alloying-dealloying process. As a result, tin titanate nanowires coupled with SnO_2 nanoparticles showed improved cycling performance, and delivered stable discharge capacity of 200 mA h/g, four times that of the aggregates of SnO_2 nanoparticles after 50 cycles. Even though this discharge capacity is still low, further improvement can be achieved by properly controlling the size, morphology of titanate precursors and the Sn content within composite structures. Besides, these structures exhibited remarkably low (<0.5 V) voltage for Li insertion electrode in lithium ion batteries.

Acknowledgements

The authors acknowledge the financial support of the City University of Hong Kong through Strategic Research Grant 7004010, Operational Program Research and Development for Innovations – European Regional Development Fund (Project No. CZ.1.05/2.1.00/03.0058), and Operational Program Education for Competitiveness-European Social Fund (CZ.1.07/2.3.00/20.0017) of the Ministry of Education, Youth and Sports of the Czech Republic. Some SEM and TEM works were done at International Center for Dielectric Research (ICDR), Xi'an Jiaotong University，Xi'an,China; The authors also thank Prof. Guang Yang for his help. This work was also supported by the Fundamental Research Funds for the Central Universities in China (Project No. 08143072).

References

1. H. Wang, L. Xi, J. Tucek, Y. Zhan, T. F. Hung, S. V. Kershaw, R. Zboril, C. Y. Chung and A. L. Rogach, *Nanoscale*, 2013, 5, 9101-9109.
2. J. Ning, T. Jiang, K. Men, Q. Dai, D. Li, Y. Wei, B. Liu, G. Chen, B. Zou and G. Zou, *J. Phys. Chem. C* 2009, 113, 14140-14144.
3. Y. H. Xu, Q. Liu, Y. J. Zhu, Y. H. Liu, A. Langrock, M. R. Zachariah and C. S. Wang, *Nano Lett.* , 2013, 13, 470-474.
4. M. V. Reddy, G. V. Subba Rao and B. V. R. Chowdari, *Chem. Rev.* , 2013, 113, 5364-5457.
5. S. Ding, D. Luan, F. Y. C. Boey, J. S. Chen and X. W. Lou, *Chem. Commun.* , 2011, 47, 7155-7157.
6. X. Wang, Z. Li and L. Yin, *CrystEngComm*, 2013, 15, 7589-7597.
7. J. M. Tarascon and M. Armand, *Nature*, 2001, 414, 359-367.
8. C. Wang, Y. Zhou, M. Ge, X. Xu, Z. Zhang and J. Z. Jiang, *J. Am. Chem. Soc.* , 2009, 132, 46-47.
9. R. Demir-Cakan, Y. S. Hu, M. Antonietti, J. Maier and M. M. Titirici, *Chem. Mater.* , 2008, 20, 1227-1229.
10. D. Deng and J. Y. Lee, *Chem. Mater.* , 2008, 20, 1841-1846.
11. X. W. Lou, Y. Wang, C. L. Yuan, J. Y. Lee and L. A. Archer, *Adv. Mater.* , 2006, 18, 2325-2329.
12. L. Y. Jiang, X. L. Wu, Y. G. Guo and L. J. Wan, *J. Phys. Chem. C* 2009, 113, 14213-14219.
13. H. Wang, F. Fu, F. Zhang, H.-E. Wang, S. V. Kershaw, J. Xu, S.-G. Sun and A. L. Rogach, *J. Mater. Chem.* , 2012, 22, 2140 - 2148.
14. Q. Han, J. Zai, Y. Xiao, B. Li, M. Xu and X. Qian, *Rsc Adv*, 2013, DOI: 10.1039/c3ra43905d.
15. Y.-H. Jin, K.-M. Min, S.-D. Seo, H.-W. Shim and D.-W. Kim, *J. Phys. Chem. C* 2011, 115, 22062-22067.
16. H.-X. Zhang, C. Feng, Y.-C. Zhai, K.-L. Jiang, Q.-Q. Li and S.-S. Fan, *Adv. Mater.* , 2009, 21, 2299-2304.
17. C. Xu, J. Sun and L. Gao, *J. Phys. Chem. C* 2009, 113, 20509-20513.
18. G. Chen, Z. Wang and D. Xia, *Chem. Mater.* , 2008, 20, 6951-6956.
19. Z. Wen, Q. Wang, Q. Zhang and J. Li, *Adv. Funct. Mater.* , 2007, 17, 2772-2778.
20. X.-M. Liu, Z. d. Huang, S. w. Oh, B. Zhang, P.-C. Ma, M. M. F. Yuen and J.-K. Kim, *Compos. Sci. Technol.* , DOI: 10.1016/j.compscitech.2011.11.019.
21. G. N. Zhu, C. X. Wang and Y. Y. Xia, *J. Power Sources* 2011, 196, 2848-2853.
22. J. R. Li, Z. L. Tang and Z. T. Zhang, *Chem. Mater.* , 2005, 17, 5848-5855.
23. N. Kumada, Y. Yonesaki, T. Takei, N. Kinomura and S. Wada, *Mater. Res. Bull.* , 2009, 44, 1298-1300.
24. V. Arantes, *J. Mater. Eng. Perform.* , 2012, 21, 1777-1784.
25. K. S. Beenakumari, *Int. J. Mater. Sci. Innov.*, 2013, 1 174-181.
26. C.-C. Tsai, L.-C. Chen, T.-F. Yeh and H. Teng, *J. Alloys Compd.* , 2013, 546, 95-101.
27. H. Wang, W. Shao, F. Gu, L. Zhang, M. Lu and C. Li, *Inorg. Chem.* , 2009, 48, 9732-9736.
28. H. Y. Zhu, Y. Lan, X. P. Gao, S. P. Ringer, Z. F. Zheng, D. Y. Song and J. C. Zhao, *J. Am. Chem. Soc.* , 2005, 127, 6730-6736.
29. H. Wang, K. Dou, W. Y. Teoh, Y. Zhan, T. F. Hung, F. Zhang, J. Xu, R. Zhang and A. L. Rogach, *Adv. Funct. Mater.* , 2013, 23, 4847-4853.

30. H. Wang, S. Kalytchuk, H. Yang, L. He, C. Hu, W. Y. Teoh and A. L. Rogach, *Nanoscale*, 2014, DOI: 10.1039/C4NR00672K.
31. H. Wang and A. L. Rogach, *Chem. Mater.* , 2014, 26, 123-133.
32. Z. Wang, D. Luan, F. Y. Boey and X. W. Lou, *J. Am. Chem. Soc.* , 2011, 133, 4738-4741.
33. R. Yang, W. Zhao, J. Zheng, X. Z. Zhang and X. G. Li, *J. Phys. Chem. C* 2010, 114, 20272-20276.
34. Z. X. Yang, G. D. Du, Q. Meng, Z. P. Guo, X. B. Yu, Z. X. Chen, T. L. Guo and R. Zeng, *Rsc Adv*, 2011, 1, 1834-1840.
35. J. C. Kim, I. S. Hwang, S. D. Seo, G. H. Lee, H. W. Shim, K. S. Park and D. W. Kim, *Nanotechnology*, 2012, 23.